*Articles*

# Crystallographic Studies of Two Alcohol Dehydrogenase-Bound Analogues of Thiazole-4-carboxamide Adenine Dinucleotide (TAD), the Active Anabolite of the Antitumor Agent Tiazofurin[†,‡]

H. Li,[§] W. H. Hallows,[§] J. S. Punzi,[§] V. E. Marquez,[∥] H. L. Carrell,[⊥] K. W. Pankiewicz,[#] K. A. Watanabe,[#] and B. M. Goldstein*[,§]

*Department of Biophysics, University of Rochester Medical Center, Rochester New York 14642, Laboratory of Medicinal Chemistry, Developmental Therapeutics Program, Division of Cancer Treatment, National Cancer Institute, NIH, Bethesda, Maryland 20892, Institute for Cancer Research, Fox Chase Cancer Center, Fox Chase Pennsylvania 19111, and Memorial Sloan-Kettering Cancer Center, New York New York 10021*

*Received July 9, 1993; Revised Manuscript Received October 12, 1993*[⊕]

ABSTRACT: Thiazole-4-carboxamide adenine dinucleotide (TAD) is the active anabolite of the antitumor drug tiazofurin. β-methylene TAD (β-TAD) is a phosphodiesterase-resistant analogue of TAD, active in tiazofurin-resistant cells. β-methylene SAD (β-SAD) is the active selenium derivative of β-TAD. Both agents are analogues of the cofactor NAD and are capable of acting as general dehydrogenase inhibitors. Crystal structures of β-TAD and β-SAD bound to horse liver alcohol dehydrogenase (LADH) are presented at 2.9 and 2.7 Å, respectively. Both complexes crystallize in the orthorhombic space group $C222_1$ and are isomorphous to apo-LADH. Complexes containing β-TAD and β-SAD were refined to crystallographic *R* values of 15% and 16%, respectively, for reflections between 8 Å and the minimum *d* spacing. Conformations of both inhibitors are similar. β-TAD and β-SAD bind to the "open" form of LADH in the normal cofactor-binding cleft between the coenyzme and catalytic domains of each monomer. Binding at the adenosine end of each inhibitor resembles that of NAD. However, the positions of the thiazole and selenazole heterocycles are displaced away from the catalytic Zn cation by ~4 Å. Close intramolecular S–O and Se–O contacts observed in the parent nucleoside analogues are maintained in both LADH-bound β-TAD and β-SAD, respectively. These conformational constraints may influence the binding specificity of the inhibitors.

Tiazofurin (2-β-D-ribofuranosylthiazole-4-carboxamide, NSC 286193) is a C-glycosyl thiazole nucleoside which has demonstrated clinical efficacy. In phase II trials, tiazofurin has induced complete hematologic remissions in several patients with end-stage acute nonlymphocytic leukemia or in myeloblastic crisis of chronic myeloid leukemia (Tricot et al., 1989, 1990). The efficacy of tiazofurin in the treatment of human leukemias appears to be related to two properties: the ability of tiazofurin to kill tumor cells and the ability to induce surviving cells to undergo maturation (Tricot et al., 1989, 1990). This differentiation-inducing action of tiazofurin has been noted in several human cell lines (Kiguchi et al., 1990; Olah et al., 1988; Sidi et al., 1989), and tiazofurin's maturation-inducing effect on the HL60 acute promyelocytic leukemia cell line has been the object of some scrutiny (Goldstein et al., 1991; Collart & Huberman, 1990; Knight et al., 1987; Wright, 1987; Lucas et al., 1983).

Both the antiproliferative and maturation-inducing effects of tiazofurin are attributed to the same biochemical effect: tiazofurin's ability to reduce intracellular guanine nucleotide pools (Collart & Huberman, 1990; Knight et al., 1987; Wright, 1987; Lucas et al., 1983; Sokoloski et al., 1986). This reduction results from inhibition of inosine monophosphate dehydrogenase (IMPd),[1] the enzyme catalyzing the rate-limiting step in the de novo synthesis of the guanine nucleotides (Jackson et al., 1975). The major IMPd inhibitor is a dinucleotide anabolite of tiazofurin. Tiazofurin is converted, via its 5′-phosphate (TrMP), into an analogue of the cofactor nicotinamide adenine dinucleotide (NAD). In this NAD analogue, called TAD (thiazole-4-carboxamide adenine dinucleotide (Figure 1), the nicotinamide ring is replaced by a thiazole-4-carboxamide moiety (Cooney et al., 1982). TAD is a more potent inhibitor of IMPd than either TrMP or tiazofurin itself (Cooney et al., 1982). Resistance to tiazofurin is associated with a decline in the synthesis of TAD accompanied by increased degradation of this active dinucleotide by a phosphodiesterase ("TADase") (Ahluwalia et al., 1987; Jayaram, 1986; Jayaram & Johns, 1986). Resistant cell lines, such as human colon carcinoma HT29, have lowered levels of anabolic

† Supported by National Cancer Institute Grants CA 45145 (B.M.G) and CA 10925 (H.L.C).

‡ Crystallographic coordinates have been deposited in the Brookhaven Protein Data Bank under file names 1ADF and 1ADG for the β-TAD and β-SAD complexes, respectively.

* To whom correspondence should be addressed.
§ University of Rochester Medical Center.
∥ National Cancer Institute.
⊥ Fox Chase Cancer Center.
# Memorial Sloan-Kettering Cancer Center.

⊕ Abstract published in *Advance ACS Abstracts*, December 1, 1993.

[1] Abbreviations: TAD, thiazole-4-carboxamide adenine dinucleotide; SAD, selenazole-4-carboxamide adenine dinucleotide; β-TAD, β-methylene thiazole-4-carboxamide adenine dinucleotide; β-SAD, β-methylene selenazole-4-carboxamide adenine dinucleotide; $H_2$NADH, 1,4,5,6-tetrahydronicotinamide adenine dinucleotide; LADH, horse liver alcohol dehydrogenase; IMPd, inosine 5′-monophosphate dehydrogenase.

0006-2960/94/0433-23$04.50/0 

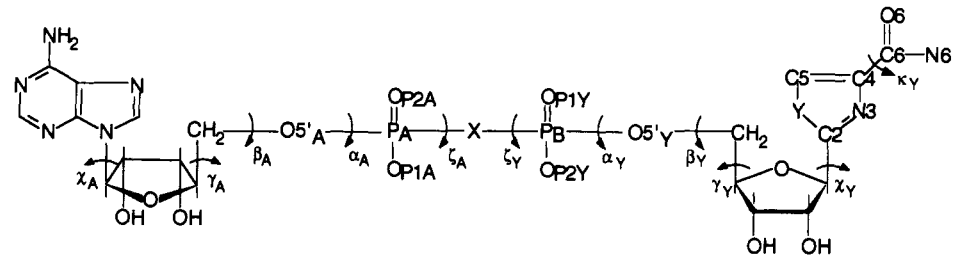

TAD : X = O, Y = S

SAD : X = O, Y = Se

β-TAD : X = $CH_2$, Y = S

β-SAD : X = $CH_2$, Y = Se

FIGURE 1: Structural formulas of the inhibitors. Atom labels are shown for the pyrophosph(on)ate group and five-membered heterocycle. Additional atom labels are adopted from those of Eklund et al. (1984). Note that the subscript "Y" refers to the thiazole or selenazole end of the molecule. Torsion angle definitions follow those of the IUPAC-IUB (IUPAC-IUB Joint Commission on Biological Nomenclature, 1983).

enzymes as well as increased levels of TADase (Jayaram, 1986; Ahluwalia et al., 1987; Jayaram & Johns, 1986). The β-methylene analogue of TAD (β-TAD, Figure 1) is resistant to this phosphodiesterase, due to replacement of the pyrophosphate oxygen with a phosphonate $CH_2$ bridge (Marquez et al., 1986). For this reason, β-TAD shows significant cytotoxicity against tiazofurin-resistant p388 (Marquez et al., 1986), L1210, and human colon carcinoma HT29 cells (H. N. Jayaram, unpublished results).

The selenium analogue of tiazofurin, selenazofurin, has also been studied. Selenazofurin is more cytotoxic than tiazofurin (Collins et al., 1977; Boritzki et al., 1985; Streeter & Robins, 1985; Jayaram et al., 1983). Selenazofurin also induces HL-60 cell maturation (Sidi et al., 1989; Lucas et al., 1983). Its corresponding dinucleotide anabolite, SAD (Figure 1), binds more tightly to IMPd than does TAD (Marquez et al., 1986; Collins et al., 1977; Boritzki et al., 1985; Streeter & Robins, 1985; Jayaram et al., 1983). The phosphodiesterase-resistant selenium analogue, β-SAD (Figure 1), is equally as effective as β-TAD in tiazofurin-resistant cell lines (H. N. Jayaram, unpublished results).

Tiazo- and selenazofurin and their derivatives have been the subject of a number of structural studies. Results suggest that certain conformational features are conserved in the thiazole and selenazole nucleosides. Crystal structures of tiazofurin (Goldstein et al., 1983) and eight inactive analogues (Goldstein et al., 1988; Burling et al., 1991, 1992; Burling & Goldstein, 1992) demonstrate a close intramolecular contact between the heterocyclic sulfur atom S and the furanose ring oxygen O4′. Observed S···O4′ distances in all cases are less than the sum of the sulfur and oxygen van der Waals radii. Similarly, the crystal structures of selenazofurin and its α-anomer show selenium–oxygen contacts which are significantly less than the sum of the selenium and oxygen van der Waals radii (Goldstein et al., 1985).

Quantum mechanical-based computational studies suggest that the close S/Se···O contacts observed in the thiazole and selenazole nucleosides are the result of an attractive electrostatic interaction between a negatively charged furanose oxygen and positively charged sulfur or selenium (Burling & Goldstein, 1992). This hypothesis is supported by $^{77}Se$ NMR studies on selenazofurin (Goldstein et al., 1990b) and by a database survey of over 400 crystal structures showing close S···O contacts (Burling & Goldstein, 1993).

The biological implications of an attractive S/Se···O interaction in the thiazole and selenazole nucleosides are important. This interaction would be expected to constrain rotation about the C-glycosidic bond in the active anabolites TAD and SAD and the phosphodiesterase-resistant derivatives β-TAD and β-SAD. Computational studies suggest that this constraint would be significant, creating a ~4 kcal/mol barrier to rotation about the C-glycosidic bond and favoring the conformation in which the base S or Se and furanose oxygen are adjacent (Burling & Goldstein, 1992). Thus, the S/Se···O interaction might be expected to influence the binding of the dinucleotide inhibitors to both the target enzyme (IMPd) and to other dehydrogenases (Goldstein et al., 1990a).

Kinetic studies show that TAD, SAD, β-TAD, and β-SAD all act as general dehydrogenase inhibitors, albeit with varying specificities (Goldstein et al., 1990a). Studies with mammalian glutamate, lactate, malate, and alcohol dehydrogenases show that, in general, the thiazole and selenazole dinucleotides bind IMPd with ~1–2 kcal/mol higher affinity (Marquez, 1986; Goldstein et al., 1990a). These studies also suggest that the inhibitors bind at the cofactor site. Nevertheless, the extent to which these inhibitors can mimic cofactor binding is expected to be limited by the S/Se···O interaction and to vary from enzyme to enzyme, depending upon the unique structural requirements of a given cofactor site.

No X-ray structure of IMPd has been obtained, thus the specific stereochemical requirements of the nicotinamide end of the cofactor binding site(s) on IMPd are unknown. However, the structural requirements for cofactor binding have been investigated in other dehydrogenases. In particular, cofactor binding to LADH has been extensively characterized (Eklund et al., 1984; Cedergren-Zeppezauer, 1986). LADH is an 80 000 Da dimer, each monomer consisting of well-defined catalytic and cofactor domains. Binding of NAD induces a conformational change in each monomer from an "open" to a "closed" form (Eklund et al., 1984; Cedergren-Zeppezauer, 1986). In the "closed" conformation, the catalytic domain rotates by about 10° relative to the coenyzme-binding domain about an axis through the central core of the protein (Colonna-Cesari et al., 1986). As a consequence, the coenzyme binding cleft between the two domains narrows. NAD binds tightly within this narrowed cleft, the nicotinamide ring anchored close to the active site by three direct hydrogen bonds between the carboxamide group and the enzyme (Eklund

et al., 1984). Initial recognition of the cofactor appears to occur via binding of the adenine end in the open conformation of the enzyme. The change to the closed form requires binding of the nicotinamide end of the cofactor, as well as coordination of the active site Zn cation by an appropriate substrate ligand (Eklund et al., 1984). LADH crystallizes in the "open" form in either the absence of cofactor (apo form) (Eklund et al., 1976), the presence of an unsuitable Zn ligand (Cedergren-Zeppezauer et al., 1982; Cedergren-Zeppezauer, 1983), and/or binding of several cofactor analogues modified at the nicotinamide end (Abdallah et al., 1975; Samama et al., 1977; Eklund et al., 1984).

Modeling studies with alcohol dehydrogenase have suggested that a thiazole dinucleotide can strictly mimic NAD binding in the closed conformation, forming the same hydrogen bonds as those stabilizing the nicotinamide carboxamide group (Goldstein et al., 1990a). However, adoption of the cofactor conformation at the nicotinamide end of the site requires a rotation about the C-glycosidic bond which significantly compromises the heteroatom–oxygen contact (Goldstein et al., 1990a). Alternatively, the inhibitor can maintain the S/Se···O interaction in the open conformation binding site, but at the expense of the other stabilizing interactions. Thus, alcohol dehydrogenase offers an excellent system in which to examine (1) whether or not the S/Se···O interaction is maintained in the enzyme-bound dinucleotide inhibitors and (2) whether or not this interaction has any influence on dehydrogenase binding by TAD, SAD, and their derivatives.

In the present study, we present the first structural determinations of enzyme-bound analogues of TAD and SAD. The structures of the phosphodiesterase-resistant analogues β-TAD and β-SAD, complexed with alcohol dehydrogenase, are determined from 2.9- and 2.7-Å data sets, respectively. These structures demonstrate that the S/Se···O interaction is maintained in the enzyme-bound species, resulting in significant deviations from normal cofactor binding at the nicotinamide end of the cofactor site.

## EXPERIMENTAL PROCEDURES

*Crystals and Data Collection.* β-TAD was prepared as described (Marquez et al., 1986). β-SAD was prepared by a similar procedure. Horse liver ADH was obtained as a crystalline suspension from Boehringer Mannheim (Indianapolis, IN). Purity was verified by electrophoresis. Protein solutions were prepared by a modification of methods described previously (Zeppezauer et al., 1967). Briefly, 10 mg of the crystalline suspension was pelleted by centrifugation, and the supernatant was discarded. The pellet was suspended in 500 μL of 50 mM Tris buffer at pH 9.4 ± 0.1 (+5 °C) and dialyzed against 20 mL of the same buffer for at least 24 h. The dissolved protein was brought to 50 mM Tris, pH 8.4 ± 0.1 (+5 °C), and 4% (v/v) precipitant by dialysis. The protein concentration was adjusted to ~20 mg/mL by ultrafiltration in a microcon 10 (Amicon, Beverly, MA). A 10-fold molar excess of inhibitor was added to the concentrated protein, and the solution was filtered through a 0.45-μm cellulose acetate filter (Costar, Cambridge, MA). LADH crystals were obtained by vapor diffusion of 4-μL hanging drops against 4–15% (v/v) ethanol (β-TAD) or 4–15% (v/v) poly(ethylene glycol) 400 (β-SAD) in 50 mM Tris, pH 8.4 ± 0.1 (+5 °C). Crystals typically appeared in 2–3 days and reached maximal size in 7 days. Typical crystal sizes were 0.1 mm × 0.2 mm × 0.5 mm. Crystals were sealed in glass capillary tubes with mother liquor for data collection.

X-ray diffraction data from both LADH–β-SAD and LADH–β-TAD crystals were collected on a Xentronics area detector with a Cu rotating anode X-ray source operating at 50 mA and 60 kV. Data were obtained from a single crystal of each complex, the crystal temperature being maintained at 4 ± 1 °C throughout the data collection. For the β-SAD complex, the detector was set at $2\theta = 25°$ with a crystal to detector distance of 19 cm. Data were obtained from a single setting using an oscillation angle of 0.25° in ω and exposure of 90 s per frame. For the β-TAD complex, the detector was set at $2\theta = 22°$ with a crystal to detector distance of 15 cm. Data were obtained from two settings using an oscillation angle of 0.25° in ω and exposure of 120 s per frame. LADH–β-TAD crystals provided useful data to 2.9 Å ($\langle I/\sigma(I)\rangle$ = 2.5). These data were processed using XDS software (Kabsch, 1988a,b). The LADH–β-SAD complex provided useful data to 2.7 Å ($\langle I/\sigma(I)\rangle$ = 1.5). Data for this complex were processed using XENGEN software (Howard et al., 1987). Crystal data and intensity statistics for both complexes are summarized in Table I. Standard deviations in cell dimensions for both complexes are estimated at ~0.1–0.2 Å, based on the variations in these parameters refined from successive blocks of data.

Table I: Crystal and Diffraction Data

| | LADH–β-SAD | LADH–β-TAD |
|---|---|---|
| crystal system | orthorhombic | orthorhombic |
| space group | $C222_1$ | $C222_1$ |
| $a$ (Å) | 56.3 | 56.3 |
| $b$ (Å) | 75.2 | 75.4 |
| $c$ (Å) | 182.3 | 181.7 |
| resolution ($d_{min}$, Å) | 2.7 | 2.9 |
| $\langle I/\sigma(I)\rangle$ up to $d_{min}$ | 1.5 | 2.5 |
| no. of reflections collected | 23350 | 22631 |
| data completeness (%) | 86 | 97 |
| $R_{merge}$ (%)[a] | 10.6 | 8.1 |

[a] $R_{merge} = \sum_{hkl}\sum_i|I^i_{hkl} - \langle I_{hkl}\rangle|/\sum_{hkl}\sum_i I^i_{hkl}$.

*Refinement.* Crystals of both complexes were isomorphous with those of native LADH (Eklund et al., 1976). Starting phases for refinement of both structures were obtained from the apoenzyme coordinates obtained at 2.4 Å (Eklund et al., 1976). Coordinates were obtained from the Brookhaven Protein Databank (Bernstein et al., 1987). All refinements were performed using the molecular dynamics program XPLOR version 3.0 (Brünger, 1992). Map display employed the program CHAIN (Sack, 1988). Refinement procedures were similar for the two complexes and are described below and summarized in Table II.

Fifteen steps of rigid body refinement were performed starting from the apostructure using data between 8 and 3 Å. (Table II). Preliminary $(|F_o|-|F_c|)e^{i\alpha calc}$ maps showed electron density at 3.5σ corresponding to the bound adenosine moiety. A 2′-endo pucker on the adenosine ribose was clearly discernable. The adenosine fragment was built into the model, and 120 steps of conjugate gradient minimization were performed (Table II). Adenosine-omitted $(|F_o| - |F_c|)e^{i\alpha calc}$ and $(2|F_o| - |F_c|)e^{i\alpha calc}$ maps now showed continuous density corresponding to the entire β-SAD molecule extending into the cofactor binding cleft. In particular, a large bulge of density at 2.5σ indicating the position of the Se atom was clearly visible. These features were less evident, but still discernable for the β-TAD structure. Densities corresponding to the sulfur and selenium atoms were used to orient the thiazole and selenazole rings in the models. Features unambiguously defining the puckering of the thiazole and selenazole riboses were not present. However, manual manipulation indicated that a 3′-endo, 2′-exo fragment best fit the electron density in both complexes, allowing formation of reasonable hydrogen

Table II: Summary of Refinement Procedures and Results for LADH–β-TAD and LADH–β-SAD Complexes

| step | $R^a$ | model | RMS values: bond length (Å) | bond angle (deg) | dihedral angle (deg) | improper torsion angle (deg) | $\chi_{S/Se}$ (deg) |
|---|---|---|---|---|---|---|---|
| (1) rigid body refinement | 0.253 | LADH (β-SAD) | | | | | |
| | 0.242 | LADH (β-TAD) | | | | | |
| (2) conjugate minimization | 0.210 | LADH + adenosine (β-SAD) | | | | | |
| | 0.200 | LADH + adenosine (β-TAD) | | | | | |
| (3) simulated annealing[b] | | | | | | | |
| $k\chi_{Se}$ = 1.1 kcal/mol | 0.167 | LADH + β-SAD | 0.016 | 3.4 | 25.8 | 2.2 | −21 |
| $k\chi_S$ = 1.1 kcal/mol | 0.159 | LADH + β-TAD | 0.017 | 3.4 | 25.9 | 2.2 | −23 |
| (4) conjugate minimization | | | | | | | |
| $k\chi_{Se}$ = 0 kcal/mol | 0.161 | LADH + β-SAD + solvent | 0.018 | 3.4 | 25.3 | 2.2 | −22 |
| $k\chi_S$ = 0 kcal/mol | 0.154 | LADH + β-TAD + solvent | 0.017 | 3.4 | 25.8 | 2.2 | −34 |

[a] Unweighted residual: $R = \sum_{hkl}[|F_o(hkl)| - k|F_c(hkl)|]/\sum_{hkl}|F_o(hkl)|$, where $k$ is the scaling factor. $R$ is calculated for all reflections between 8 Å and $d_{min}$, except for step 1 (see Experimental Procedures). [b] $k\chi_{Se/Se}$ is the force constant in the dihedral angle energy term used for the C-glycosidic torsion angle: $E = k\chi_{S/Se}[1 + \cos(2\chi_{S/Se} + 180°)]$ (see Experimental Procedures).

bonds between the ribose hydroxyls and residues 269 and 47. This pucker is observed in the nicotinamide ribose of free Li-NAD$^+$ (Reddy et al., 1981). Given the limitations imposed by the resolutions of the data sets, sugar puckers were restrained in subsequent annealing cycles (below) to 2′-endo for the adenine ribose ($P$ = 159°, $^2E$) and 3′-endo, 2′-exo ($P$ = −6°, $^3{}_2T$) for the thiazole and selenazole riboses. However, no significant differences in either average thermal factors or map features were observed between restrained and nonrestrained models.

Force parameter and topology files for simulated annealing of the β-TAD and β-SAD complexes were obtained by modifying existing XPLOR parameter and topology files for the NAD$^+$ molecule. Files are listed in the supplementery material. Electronic charges for the thiazole and selenazole rings were taken from previous *ab initio* calculations (Burling & Goldstein, 1992). A Cambridge Database search (Version 4.5; Allen et al., 1983) was used to determine equilibrium values for the P–C bond length (1.789 Å) and P–C–P angle (116°) in the β-methylene linkage. Planarity of the five-membered heterocycle and attached carboxamide group was restrained.

The dihedral angle energy term for the C-glycosidic torsion angle $\chi_{S/Se}$(O4′$_Y$–C1′$_Y$–C2$_Y$–S/Se) was defined as

$$E = k\chi[1 + \cos(n\chi + \delta)]$$

where $n$ = 2 and $\delta$ = 180°. The force constant for the C-glycosidic torsion angle of β-SAD, $k\chi_{Se}$, was set at several different values to examine its effects on the conformation around the C-glycosidic bond. Two values were examined for $k\chi_{Se}$: 1.1 and 0.5 kcal/mol, other parameters remaining unchanged. The entire LADH–β-SAD complex was then subjected to the same simulated annealing procedure, using each of the two force constants. Resulting values of $\chi_{Se}$ were within 10°, suggesting that the magnitude of $k\chi_{Se}$ did not substantially influence the annealed conformation around the C-glycosidic bond. Results are reported in Table II for the 1.1 kcal/mol value subsequently used. Only a single value of the corresponding force constant $k\chi_S$ was used for β-TAD due to the lower resolution of the data (Table II). Following the simulated annealing procedure, the restraint on the C-glycosidic bond was released in both complexes ($k\chi_{Se/S}$ = 0.0 kcal/mol). Subsequent conjugate gradient refinement (below) produced little change in $\chi_{Se}$ or $\chi_S$.

Simulated annealing was performed as follows. The system was initially heated to 2000 K and slowly cooled to 300 K in 25 K steps. At each temperature, a 25-fs molecular dynamics run was performed using the $T$ coupling strategy (Brünger et al., 1990), followed by 120 steps of conjugate gradient minimization. Ten steps of overall $B$-factor refinement were then performed followed by 20 steps of individual $B$-factor refinement. $R$ values were reduced to 15.9% for β-TAD data between 8 and 2.9 Å and 16.7% for β-SAD data between 8 and 2.7 Å.

Table III: List of Atom Pairs within 3.2 Å between β-TAD or β-SAD and LADH

| LADH | β-TAD/β-SAD | D (Å)[a] | type of contact[a] |
|---|---|---|---|
| Arg-47 NE | O3′$_Y$[b] | 2.7/2.9 | H-bond |
| Arg-47 CG | O3′$_Y$ | 3.2/3.5 | VDW |
| Arg-47 CD | O3′$_Y$ | 3.1/3.6 | VDW |
| His-51 NE2 | N6$_Y$ | 2.9/3.7 | H-bond/VDW |
| Gly-202 N | O$_{P1Y}$ | 3.0/3.2 | H-bond |
| Val-203 N | O$_{P1Y}$ | 3.1/3.2 | H-bond |
| Asp-223 OD1 | O2′$_A$ | 2.6/2.8 | H-bond |
| Asp-223 OD2 | O3′$_A$ | 2.9/2.8 | H-bond |
| Lys-228 NZ | O3′$_A$ | 2.6/2.8 | H-bond |
| Val-268 O | O4′$_Y$ | 3.0/3.1 | VDW |
| Ile-269 O | O2′$_Y$ | 3.1/3.1 | H-bond |
| Ile-269 O | C1′$_Y$ | 2.9/2.7 | VDW |
| Val-294 CA | N6$_Y$ | 3.1/3.2 | VDW |
| Val-294 O | N6$_Y$ | 3.4/2.8 | VDW/H-bond |
| Pro-295 N | N6$_Y$ | 3.6/3.2 | VDW/H-bond |
| Pro-295 CA | N6$_Y$ | 3.2/3.2 | VDW |
| W501 O | O6$_Y$ | 3.2/2.8 | H-bond |

[a] Distances and interactions are listed in the order β-TAD/β-SAD. [b] Y = S or Se.

At this stage ($|F_o| - |F_c|$)$e^{i\alpha calc}$ and ($2|F_o| - |F_c|$)$e^{i\alpha calc}$ maps were used to examine the refined structure, add ordered water molecules, and identify hydrogen bonds. The criteria for adding a water molecule were (1) the presence of a peak on the ($|F_o| - |F_c|$)$e^{i\alpha calc}$ map at the 2.5$\sigma$ level, (2) the presence of a peak at the same location on the ($2|F_o| - |F_c|$)$e^{i\alpha calc}$ map at the 1$\sigma$ level, and (3) the presence of a reasonable hydrogen-bonding geometry between the putative solvent and a protein residue, the inhibitor, and/or another water molecule. Thirty-four peaks in the LADH–β-TAD model and 52 peaks in LADH–β-SAD fit these criteria. Hydrogen bonds were assigned on the basis of continuous density between the inhibitors and protein. Distances between hydrogen-bond donors and acceptors, and other close contacts, are listed in Table III.

Unaccountable, but weak density in the diphosphate regions of both inhibitors suggested the possibility of minor alternative conformations for the β-methylene chains. However, attempts at refining positional disorder models yielded unreasonable binding geometries and were not pursued.

Neither data set was of sufficient resolution to assign the conformation of the thiazole or selenazole carboxamide groups.

However, both small molecule crystal structures and *ab initio* calculations strongly suggest that the orientation of this group with respect to the thiazole and selenazole heterocycles is constrained such that the carboxamide amino group is ~*cis* planar to the heterocyclic nitrogen (Li & Goldstein, 1992). The final conformation of the carboxamide groups of both ligands was inferred from this constraint and from the protein environment. However, refinement of the two complexes converged to two slightly different carboxamide group conformations, regardless of starting orientations. In the β-SAD complex, annealing maintained the carboxamide group in its *cis*-planar orientation ($\kappa \sim 0°$). This model places $N6_S$ 3.2 Å from the main chain nitrogen of Pro-295 and 2.8 Å from the carbonyl oxygen of Val-294 O. In the β-TAD complex, rotation of the carboxamide group by ~20° out of the plane of the thiazole ring brought the amide group within 2.9 Å of NE2 of His-51. This model requires a 180° rotation of the histamine ring relative to that in the β-SAD model, as well as deprotonation at NE2. Rotation of His-51 in the β-TAD model brings the CD2 carbon to within 2.8 Å of a solvent molecule. In the β-SAD model, this position on the ring is occupied by ND1, which hydrogen bonds to this water.

These models, with solvent, were subjected to a repetitive refinement procedure consisting of a 120-step conjugate gradient minimization and 35-step *B*-factor refinement. The final *R* factor converged to 15.4% for LADH–β-TAD (8–2.9 Å data) and 16.1% for LADH–β-SAD (8–2.7 Å data). Final RMS values are summarized in Table II.

## RESULTS

### *LADH Structure*

Electron density maps show unambiguously the position of the protein backbone. On the protein surface, where the structure tends to be more flexible, electron density for some side chains is weak or missing. Luzzati plots (Luzzati, 1952) of the final refined models (supplementary material) indicate an average positional error of ~0.3 Å in both LADH–β-SAD and LADH–β-TAD. These assume that positional errors are the sole source of differences in $F_o$ and $F_c$ and that these errors are normally distributed (Luzzati, 1952). Ramachandran plots (Ramachandran & Sasisekharan, 1968) (supplementary material) indicate that the majority of $\psi/\phi$ angles for the non-glycine residues are reasonable. Most glycine residues are poorly defined given the limited resolutions of the structures. RMS deviations between refined models from ideal geometries are indicated in Table II. The RMS deviation between the protein backbones in the two complexes is 0.34 Å. The RMS deviation between the two proteins with side chains is 0.78 Å.

In both complexes, the protein crystallizes in the "open" conformation seen in the apo form (Eklund et al., 1976). Comparison of protein backbones between apo-LADH and LADH in the β-SAD complex gives a RMS deviation of 0.37 Å. Comparison of both backbones and side chains gives a RMS deviation of 0.79 Å. In general, side chains have larger RMS differences than backbones. The largest deviation is seen in the sidechain of Arg-47 (3.2 Å). The position of this side chain is not well-defined in the apoenzyme (Eklund et al., 1976) but was positioned in the cofactor binding cleft in that model. Upon binding of β–SAD or β-TAD, Arg-47 is displaced from the cleft, forming a hydrogen bond to the O3′ hydroxyl group of the thiazole and selenazole riboses (below). The final density of Arg-47 is well-defined in both LADH–β-TAD and LADH–β-SAD.

In both refined complexes, a consistent, well-defined peak in the difference map is observed about 2 Å from the active site zinc atom, indicating a coordinating solvent molecule. This density is located at the putative substrate binding site (Cedergren-Zeppezauer et al., 1982; Eklund et al., 1982a,b, 1984). Ethanol was present as preciptant in the LADH–β-TAD crystal. However, given the moderate resolution of the data, no attempt was made to model ethanol at the Zn site in this complex. In the final models of both complexes, this Zn coordination ligand is occupied by a water molecule.

### *β-TAD/β-SAD Binding to ADH*

*General Features.* Inhibitor-omitted $(|F|_o - |F_c|)e^{i\alpha_{calc}}$ maps in the region of the cofactor binding cleft are shown for the refined β-TAD and β-SAD complexes in Figure 2. In both complexes, the ligands bind in extended conformations to the open form of the enzyme. The conformations of LADH-bound β-TAD and β-SAD are quite similar (Figure 3). The RMS deviation between the two ligands is 0.4 Å. As expected, the greatest differences between the two ligands are seen in the region of the five-membered heterocycle. The larger selenazole ring is shifted by ~0.7 Å deeper into the binding cleft (below). Coordinates for the bound ligands and associated thermal parameters are given in the supplementary material.

Backbone torsion angles for the two ligands are given in Table IV. These are compared to values observed for NADH in the ternary complex with dimethyl sulfoxide (Eklund et al., 1984). Torsion angles are also given for the 1,4,5,6-tetrahydronicotinamide analogue of NAD ($H_2$NADH) in the ternary orthorhombic complex with methylpentanediol (MPD) (Cedergren-Zeppezauer et al., 1982). These conformations are also compared in Figure 4. The NADH conformation illustrated is that observed for cofactor bound to the closed form of the enzyme. The $H_2$NADH conformation illustrates that observed for a cofactor analogue bound to the open form.

A temperature factor gradient is seen along the length of the inhibitors, consistent with the binding modes observed in the different regions. In general, the adenine moieties show the lowest *B* values (~15–17 Å$^2$). These are "locked" into a narrow cleft in the cofactor domain (below). Temperature factors for the thiazole and selenazole ends are higher (~20–28 Å$^2$). These reside in the widened solvent-accessible cleft between the catalytic and cofactor domains seen in the open form of the enzyme (below). Larger *B* values in the regions of the phosphate chains (~26–32 Å$^2$) are also consistent with a minor degree of positional disorder (see Experimental Procedures). Ligand temperature factors do not change significantly upon release of constraints.

*Adenosine Binding.* Interactions between the ligands and the protein at the adenosine ends are very similar to those seen in LADH-bound NADH. Although NADH binds in the closed form of the enzyme, the adenosine binding end of the cofactor cleft is primarily within the cofactor domain. Thus, residues that interact with this end of the cofactor are minimally affected by the rotation of the catalytic domain relative to the cofactor domain involved in the transition to the closed form (Cedergren-Zeppezauer et al., 1982).

As in NADH binding (Eklund et al., 1984), the adenine rings in β-TAD and β-SAD lie between the side chains of residues Ile-224 and -269, in van der Waals contact with both (Figure 5). The adenine riboses of β-TAD and β-SAD are also bound in the same manner as that of the normal cofactor. Riboses at this end of the inhibitors clearly show 2′-endo puckers (see Experimental Procedures), close to those seen in

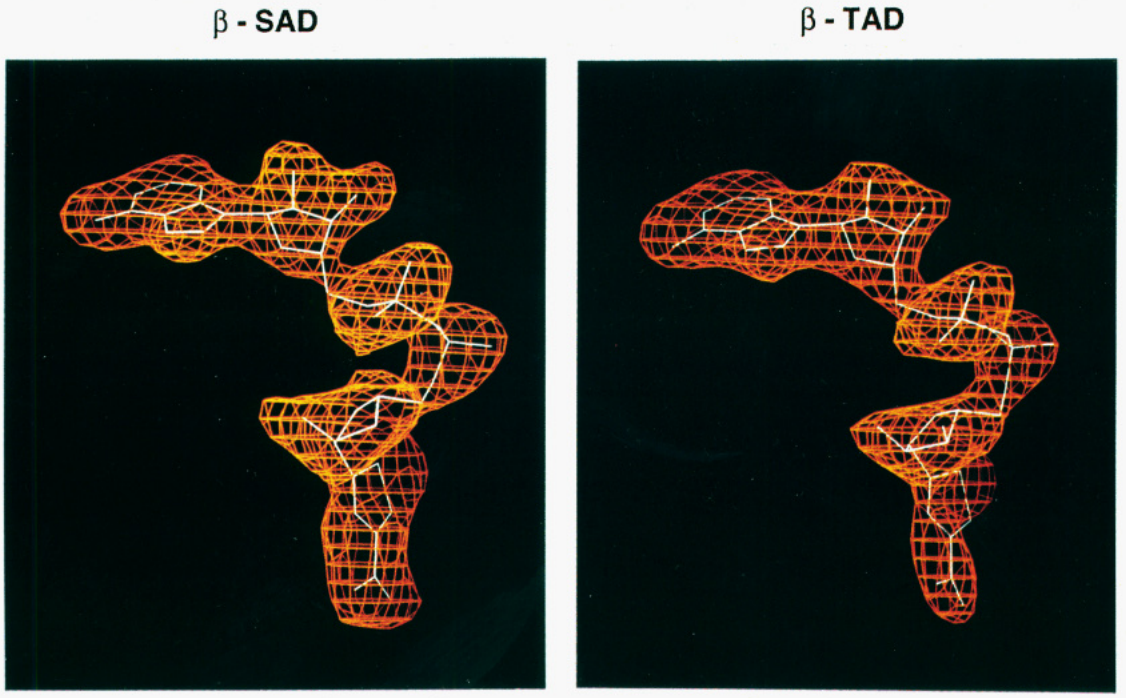


FIGURE 2: $|F_o| - |F_c|$ maps of the ligand-binding region of LADH-$\beta$-SAD (left) and LADH-$\beta$-TAD (right). Calculated structure factor amplitudes and phases were obtained from the final refined LADH models with the inhibitors omitted. Maps are contoured in red at the 2.5$\sigma$ (left) and 2.3$\sigma$ (right) level. Inhibitor models are shown in white.

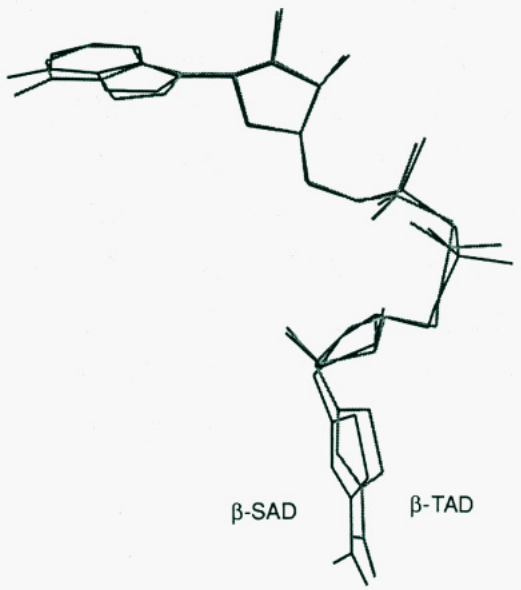


FIGURE 3: Comparison between the conformations of LADH-bound $\beta$-TAD (light bonds) and $\beta$-SAD (dark bonds). The figure was generated from a least-squares fit of the protein backbones in the two complexes.

Table IV: Conformations of $\beta$-TAD, $\beta$-SAD, $H_2NADH$, and NADH Bound to Horse Liver Alcohol Dehydrogenase

| torsion angles[a] | $\beta$-TAD | $\beta$-SAD | $H_2NADH$[b] (orthorhombic) | NADH[c] (triclinic) |
|---|---|---|---|---|
| $\chi_A$ = $C4_A$–$N9_A$–$C1'_A$–$C2'_A$ | 150 | 147 | 148 | 141 |
| $\gamma_A$ = $C3'_A$–$C4'_A$–$C5'_A$–$O5'_A$ | –83 | –77 | –109 | –89 |
| $\beta_A$ = $C4'_A$–$C5'_A$–$O5'_A$–$P_A$ | 109 | 94 | 97 | 141 |
| $\alpha_A$ = $C5'_A$–$O5'_A$–$P_A$–X | –177 | 167 | 148 | 105 |
| $\zeta_A$ = $O5'_A$–$P_A$–X–$P_Y$ | –2 | 15 | 79 | 84 |
| $\zeta_Y$ = $O5'_Y$–$P_Y$–X–$P_A$ | –94 | –98 | –61 | –152 |
| $\alpha_Y$ = $C5'_Y$–$O5'_Y$–$P_Y$–X | –5 | –12 | –122 | 68 |
| $\beta_Y$ = $C4'_Y$–$C5'_Y$–$O5'_Y$–$P_Y$ | 83 | 88 | 99 | –157 |
| $\gamma_Y$ = $C3'_Y$–$C4'_Y$–$C5'_Y$–$O5'_Y$ | 160 | 170 | –39 | 40 |
| $\chi_Y$ = $O4'_Y$–$C1'_Y$–Z–Q | –34 | –22 | –19 | 76 |
| $\chi'_Y$ = $O4'_Y$–$C1'_Y$–Z–Q' | 144 | 156 | 159 | –104 |

[a] For $\beta$-TAD and $\beta$-SAD, X = $C_{P3}$; Y = S or Se; Z = $C2_Y$; Q = S or Se and Q' = $N3_Y$ (see Figure 1). For $H_2NADH$ and NADH, X = $O_{P3}$; Y = N; Z = $N1_N$; Q = $C6_N$ and Q' = $C2_N$. [b] Cedergren-Zeppezauer et al. (1982). [c] Eklund et al. (1984). Values are averages from two cofactors related by noncrystallographic symmetry.

other dehydrogenase–cofactor complexes (Eklund & Brändén, 1987). The adenine riboses sit at the surface of the coenzyme binding domain at the point where the cofactor binding cleft turns between the coenzyme and catalytic domains. As with NADH, Asp-223 forms hydrogen bonds with both the O2′ and O3′ hydroxyl oxygen on each inhibitor ribose. Lys-228 hydrogen bonds with the O3′ hydroxyl (Table III; Figure 5). The same mode of adenosine binding is seen in other LADH complexes, including those with ADP-ribose (Eklund et al., 1984) as well as $H_2NADH$ (Cedergren-Zeppezauer et al., 1982). The structural conservation of Asp-223 among different dehydrogenases and its importance in adenine binding are well known (Eklund et al., 1984; Eklund & Brändén, 1987). This suggests that preservation of the hydrogen-bonding functionality of the adenine ribose in the thiazole and selenazole dinucleotides is necessary for activity.

*Pyrophosphonate Binding.* The pyrophosphonate group of each inhibitor binds in the cofactor cleft between the coenzyme and catalytic domains. This portion of the cofactor binding region is 2–4 Å wider in the open form of the enzyme than in the closed form, allowing significant variation in phosphate binding (Cedergren-Zeppezauer et al., 1982; Eklund et al., 1982a,b, 1984). Conformations along the adenine end of the chain in the $\beta$-methylene analogues are qualitatively similar to pyrophosphate conformations observed in previous open- and closed-form complexes (Table IV; Figure 4). The only intermolecular hydrogen bonds to the phosphonate oxygens in the $\beta$-methylene analogues are split bonds between $O_{P1Y}$ and the main chain nitrogens of Gly-202 and Val-203 (Figure 5). Similar interactions involving these residues are observed in the $H_2NADH$ complex (Cedergren-Zeppezauer et al., 1982). Arg-369 plays a major role in phosphate binding in closed-form complexes (Eklund et al., 1984). This residue

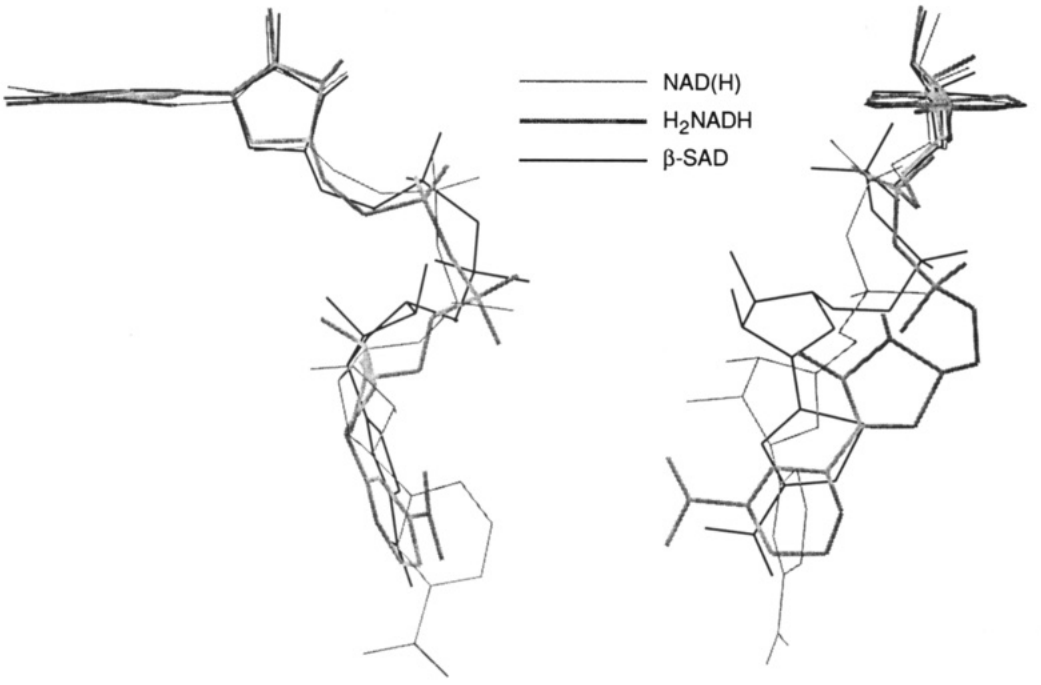


FIGURE 4: Comparison between the conformations of LADH-bound β-SAD (thin dark bonds), NADH (thin light bonds), and $H_2$NADH (thick gray bonds). The two views are related by an approximately 90° rotation about the vertical axis. The figure was generated from a least-squares fit between the adenosine ends of each ligand. The $H_2$NADH conformation is from the orthorhombic complex with MPD (Cedergren-Zeppezauer et al., 1982). The NADH conformation is from the triclinic complex with DMSO (Eklund et al., 1984; Brookhaven Protein Data Bank entry 8ADH).

does not participate in any direct interactions with the β-methylene compounds. This is also seen in the open-form $H_2$NADH complex (Cedergren-Zeppezauer et al., 1982).

Differences in conformations between the phosphate and phosphonate chains become apparent beyond the β-methylene and ester linkages (Table IV; Figure 4). Differences in conformation may result from the presence of the more acutely angled $CH_2$ bridge, as well as constraints on the thiazole and selenazole ribose conformations (below). It has been argued that steric considerations are less important than electronic effects in accounting for functional differences in phosphonate nucleotide analogues (Blackburn et al., 1981, 1985). Neither the methylene group in the inhibitors nor the phosphate ester oxygen in NAD participate in any direct LADH–ligand interactions (Eklund & Brändén, 1987). Thus, any electronic perturbation by the $CH_2$ group would need to occur via a change in polarization of the phosphate oxygens.

*Thiazole and Selenazole Nucleoside Regions.* The thiazole and selenazole ribose moieties were best modeled with 3′-endo 2′-exo ($^3_2$T) puckers (see Experimental Procedures). Nicotinamide riboses in most other LADH–ligand complexes demonstrate 2′-endo puckers (Cedergren-Zeppezauer et al., 1982; Eklund et al., 1984). In each inhibitor, the 3′-hydroxyl oxygen forms an intramolecular hydrogen bond with $O_{P1A}$ and an intermolecular bond with the NE of Arg-47. The O2′ hydroxyl oxygen forms a hydrogen bond to the carbonyl oxygen of Ile-269 (Figure 5). This is in contrast to the open-form $H_2$NADH and ADP-ribose complexes, in which the carbonyl oxygen of Ile-269 hydrogen bonds to O3′ of the nicotinamide ribose (Cedergren-Zeppezauer et al., 1982; Eklund et al., 1984). Thus, both the conformation and orientation of the thiazole and selenazole riboses are different from those of the nicotinamide riboses in other open-form complexes (Figure 4).

Given the potential constraints imposed by S/Se–O interactions in the bound ligands, conformations around the glycosidic bonds are of particular interest. C-glycosidic torsion angles $\chi_{S/Se}$(O4′–C1′–C2–S/Se) are −34° and −22° for β-TAD and β-SAD, respectively (Table IV). These conformations maintain close S/Se–O contacts similar to those observed in the small molecule crystal structures of the parent nucleosides and their analogues. The analogous values of χ in the small molecule structures are generally positive (Burling & Goldstein, 1992). However, the values observed here are equally close to the global energy minimum for the heteroatom–oxygen interaction (Burling & Goldstein, 1992). S/Se–O4′ distances in LADH-bound β-TAD and β-SAD are 2.8 and 2.6 Å, respectively. These are shorter than the S–O and Se–O distances observed in tiazofurin and selenazofurin, respectively (Burling & Goldstein, 1992).

Conformations about the C-glycosidic bonds in β-TAD and β-SAD differ by ~100° from the analogous N-glycosidic bond conformation observed in the closed-form complex of LADH-bound NADH (Table IV). The thiazole and selenazole-4-carboxamide groups are displaced ~3 Å farther away from the catalytic Zn cation relative to the normal cofactor binding position. This places the heterocycles in roughly the same region of the binding pocket as that of the tetrahydronicotinamide ring in the open-form $H_2$NADH complex (Cedergren-Zeppezauer et al., 1982) (Figure 4). The C-glycosidic torsion angles observed in β-TAD and β-SAD are similar to the N-glycosidic torsion angle in $H_2$NADH bound in this open form (Table IV). However, the thiazole and selenazole carboxamide groups occupy different positions from that of the tetrahydronicotinamide carboxamide moiety (Figure 4).

In LADH-bound β-TAD and β-SAD, the carboxamide group points toward the bottom of the binding cleft between the cofactor and catalytic domains (Figure 5). In this orientation, the carboxamide oxygen of both ligands hydrogen bonds to a water molecule. This water is part of an ordered solvent array at the bottom of the widened binding cleft. In

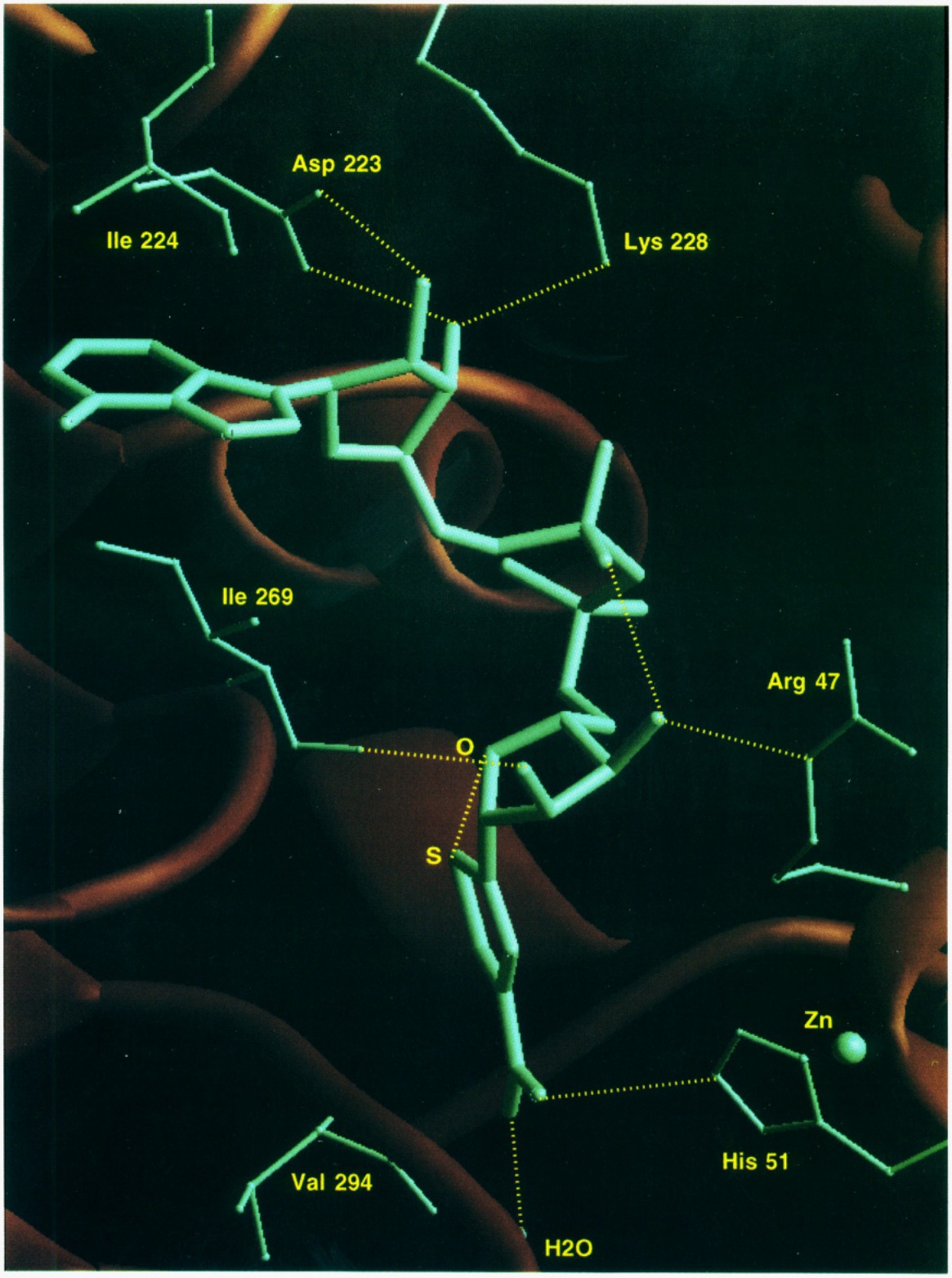


FIGURE 5: Intra- and intermolecular interactions in LADH-bound β-TAD. The ligand is in cyan. Hydrogen bond and S–O4′ interactions are represented by dotted yellow lines. Side chain and backbone atoms which interact with the ligand are shown as thin cyan bonds. Side chains of Ile-224 and Ile-269 are in van der Waals contact with the adenine ring. In β-SAD the carboxamide nitrogen interacts with the carbonyl oxygen of Val-294 instead of with His-51 (rendered with the program Ribbons; Carson, 1987).

β-TAD, the carboxamide amino group points toward His-51 in the cofactor domain, forming a hydrogen bond with NE2 of His-51 (Figure 5) (see Experimental Procedures). In the β-SAD complex, the slightly longer Se–C bonds shift the selenazole carboxamide group ~0.7 Å farther away from His-51. In this position, the carboxamide amino group is brought within 2.8 Å of the carbonyl oxygen of Val-294.

## DISCUSSION

Crystallographic and computational studies suggest that an attractive S/Se–O4′ interaction constrains rotation about the C-glycosidic bond in the thiazole and selenazole nucleoside antitumor agents tiazufurin and selenazofurin. The present structures suggest that a similar constraint exists in the active

dinucleotide anabolites TAD and SAD and their phosphodiesterase-resistant analogues β-TAD and β-SAD. The conformations of LADH-bound β-TAD and β-SAD preserve the S/Se–O4′ interaction. As a result, β-TAD and β-SAD do not strictly mimic binding of the normal cofactor NAD and do not induce the transition from the open to the closed form of the enzyme.

Binding at the adenosine ends of the inhibitors closely mimics that of NAD in the cofactor domain. As noted, other LADH-bound inhibitors with modifications at the nicotinamide end also mimic NAD binding at the adenosine site (Eklund et al., 1984; Cedergren-Zeppezauer et al., 1982; Samama et al., 1977). This occurs despite wide variations in conformation at the modified nicotinamide end. Thus, the structures reported here support the contention that initial recognition of the cofactor occurs at the adenosine binding site in the open conformation (Eklund et al., 1984).

Binding at the thiazole and selenazole ends of the inhibitors is distorted from that observed for NAD in the closed form. Differences in the phosphonate conformation, sugar puckering, and C-glycosidic torsion angle are all observed. In particular, the conformation about the C-glycosidic bonds in these inhibitors differs by ~100° from that found in the closed form of LADH-bound NAD.

Proper binding of the nicotinamide end of NAD to LADH is required to induce the conformational change from the open to the closed form of the enzyme (Eklund et al., 1984). In the closed conformation, the nicotinamide carboxamide group forms hydrogen bonds with residues Ala-317, Val-292, and Phe-319 at the end of the cofactor pocket in the catalytic domain (Eklund et al., 1984). Modeling studies show that this pocket can accommodate the inhibitor heterocycles, which can form the same hydrogen bonds as those formed by the nicotinamide ring. (Goldstein et al., 1990a). However, the constraints imposed by the S/Se–O4′ interactions would prevent the inhibitors from adopting the conformation required by the nicotinamide end of the cofactor site.

LADH binding by β-TAD and β-SAD most closely approximates that of $H_2$NADH in its ternary orthorhombic complex with MPD (Cedergren-Zeppezauer et al., 1982). In this complex, the conformations at the end of the pyrophosphate chain and about the tetrahydronicotinamide N-glycosidic bonds are also distorted from those observed in NAD in the closed-form complex. However, the pyrophosphate and N-glycosidic bonds are flexible. Thus, $H_2$NADH is capable of adopting the conformation required to induce the transition to the closed form. This is illustrated by the structure of the triclinic $H_2$NADH complex containing the substrate analogue *trans*-4-(*N*,*N*-dimethylamino) cinnamaldehyde (DACA) (Cedergren-Zeppezauer et al., 1982). In this structure, the enzyme is in the closed form, with $H_2$NADH closely mimicking the binding of NAD. This complex demonstrates that a neutral isosteric analogue of NAD can successfully mimic normal cofactor binding to LADH.

In addition to the correct cofactor conformation, the transformation from the open to the closed form of LADH requires a suitable ligand for the fourth coordination site on the catalytic zinc ion (Cedergren-Zeppezauer et al., 1982; Eklund et al., 1982a,b, 1984). This is usually provided by the alcohol substrate. In the closed-form $H_2$NADH complex, this coordination site is occupied by the substrate analogue DACA. Failure of the orthorhombic $H_2$NADH complex to adopt the closed form is attributed to the presence of MPD at the substrate site, which does not coordinate with the active site metal (Cedergren-Zeppezauer et al., 1982). In fact, binding of the inhibitor imidazole to the active site zinc maintains LADH in the open form even in the presence of NAD itself (Cedergren-Zeppezauer, 1983). In this structure, the conformation of the normal cofactor is distorted relative to that observed in the closed-form complex.

Thus, it is possible that the distortions observed in the β-SAD and β-TAD structures are not simply the result of constraints imposed by an S/Se–O4′ contact. Lack of an appropriate zinc ligand could prevent the change to the closed form of the enzyme. This in turn would distort inhibitor binding, as seen in both the $H_2$NADH–MPD and NAD–imidazole complexes.

However, a significant amount of ethanol was present in the β-TAD crystallization medium. This suggests that lack of a suitable Zn ligand is an unlikely source for the observed distortion, at least in this complex. The fourth coordination ligand in both complexes is occoupied by solvent, although it is not possible to distinguish ethanol from water at these resolutions. In either case, it is likely that constrained rotation about the C-glycosidic bond in β-SAD and β-TAD contributes to the maintenance of the open conformation in these LADH complexes. This constraint would also be expected to influence the binding of the thiazole and selenazole inhibitors to other dehydrogenases.

Conformational studies of dehydrogenase–cofactor complexes indicate that NAD is a flexible molecule (Eklund & Brändén, 1987). In particular, the conformation about the nicotinamide glycosidic bond adopts a wide range, depending upon the local interactions at the binding site. It has been noted that the conformation of the nicotinamide ring is generally *anti* in A-side-specific enzymes and *syn* in B-side-specific enzymes (Eklund & Brändén, 1987; Wu & Houk, 1991). However, there are considerable variations in nicotinamide glycosidic bond conformation, even within these classes (Eklund & Brändén, 1987).

The flexibility about the analogous C-glycosidic bond in the thiazole and selenazole dinucleotides is constrained by the intramolecular S/Se–O4′ interaction. In principle, this constraint can enhance as well as impede dehydrogenase binding by TAD, SAD, and their analogues. The outcome will depend upon the specific stereochemical requirements of the cofactor site. If the constrained conformation is that required by the nicotinamide end of the cofactor site, the inhibitor will enjoy both entropic and enthalpic advantages over the normal cofactor. The thiazole and selenazole dinucleotides do show enhanced affinity and specificity for the target enzyme IMPd (Marquez, 1986; Goldstein et al., 1990a). Identification of a potential role for the S/Se–O interaction in IMPd binding will await further studies. However, the current structures demonstrate that this nonbonded interaction is of sufficient magnitude to be maintained in enzyme-bound ligands.

## ACKNOWLEDGMENT

This paper is dedicated to the memory of Henry Katz.

## SUPPLEMENTARY MATERIAL AVAILABLE

Five figures and two tables showing Luzzati plots and Ramanchandran plots from the LADH–β-SAD and LADH–β-TAD structures, Cartesian coordinates and *B* factors for LADH-bound β-SAD and β-TAD, force parameter and topology files for β-SAD and β-TAD, and stereoviews of Figure 4 (20 pages). Ordering information is given on any current masthead page.

## REFERENCES


Abdallah, M. A., Biellmann, J.-F., Nordström, B., & Brändén, C.-I. (1975) *Eur. J. Biochem. 50*, 475–481.

Ahluwalia, G. S., Jayaram, H. N., & Cooney, D. A. (1987) in*Concepts, Clinical Developments, and Therapeutic Advances in Cancer Chemotherapy* (Muggia, F. M., Ed.) pp 63–102, Martinus Nijhoff, Boston, MA.

Allen, F. H., Kennard, O., & Taylor, R. (1983) *Acc. Chem. Res. 16*, 146–153 and references therein.

Altona, C., & Sundaralingam, M. (1972) *J. Am. Chem. Soc. 94*, 8205–8212.

Appa Rao, G. V. N., Seshasayee, M., Aravamudan, G., & Sowrirajan, S. (1983) *Acta Crystallogr. C39*, 620–622.

Bernstein, F. C., Koetzle, T. F., Williams, G. J. B., Meyer, E. F., Brice, M. D., Rodgers, J. R., Kennard, O., Shimanoudhi, T., & Tasumi, M. (1977) *J. Mol. Biol. 112*, 535–542.

Blackburn, G. M., England, D. A., & Kolkmann, F. (1981) *J. Chem. Soc., Chem. Commun.* 930–932.

Blackburn, G. M., Eckstein, F., Kent, D. E., & Perrée, T. D. (1985) *Nucleosides Nucleotides 4*, 165–167.

Boritzki, T. J., Berry, D. A., Besserer, J. A., Cook, P. D., Fry, D. W., Leopold, W. R., & Jackson, R. C. (1985) *Biochem. Pharmacol. 34*, 1109–1114.

Brünger, A. T. (1992) *X-PLOR version 3.0 Manual*, Yale University, New Haven, CT.

Brünger, A. T., Krukowski, A., & Erickson, J. W. (1990) *Acta Crystallogr. A46*, 585–593.

Burling, F. T., & Goldstein, B. M. (1992) *J. Am. Chem. Soc. 114*, 2313–2320.

Burling, F. T., & Goldstein, B. M. (1993) *Acta Crystallogr. B49*, 738–744.

Burling, F. T., Gabrielsen, B., & Goldstein, B. M. (1991) *Acta Crystallogr., Sect. C, C47*, 1272–1275.

Burling, F. T., Hallows, W. H., Phelan, M. J., Gabrielsen, B., & Goldstein, B. M. (1992) *Acta Crystallogr. B48*, 677–683.

Carson, M. (1987) *J. Mol. Graphics 5*, 103–106.

Cedergren-Zeppezauer, E. (1983) *Biochemistry 22*, 5761–5772.

Cedergren-Zeppezauer, E. (1986) in *Zinc Enzymes* (Bertini, I., Luchinat, C., Maret, W., & Zeppezauer, M., Ed.) Chapter 29, Birkhäuser, Boston.

Cedergren-Zeppezauer, E., Samama, J. P., & Eklund, H. (1982) *Biochemistry, 21*, 4895–4908.

Collart, F. R., & Huberman, E. (1990) *Blood 75*, 570–576.

Collins, S. J., Gallo, R. C., & Gallagher, R. E. (1977) *Nature 270*, 347–349.

Colonna-Cesari, F., Perahia, D., Karplus, M., Eklund, H., Brändén, C. I., & Tapia, O. (1986) *J. Biol. Chem. 261*, 15273–15280.

Cooney, D. A., Jayaram, H. N., Gebeyehu, G., Betts, C. R., Kelley, J. A., Marquez, V. E., & Johns, D. G. (1982) *Biochem. Pharmacol. 31*, 2133–2136.

Dupont, P. L., Dideberg, O., & Jacquemin, P. (1990) *Acta Crystallogr. C46*, 484–486.

Eklund, H., & Brändén, C.-I. (1987) in *Pyridine Nucleotide Coenzymes. Chemical, Biochemical, and Medical Aspects* (Dolphin, D., Avramovic, O., & Poulson, R., Eds.) Vol. II, Part A, Chapter 4, John Wiley and Sons, New York.

Eklund, H., Nordstrom, B., Zeppezauer, E., Soderlund, G., Ohlsson, I., Boiwe, T., Soderberg, B. O., Tapia, O., Brändén, C. I., & Akeson, Å. (1976) *J. Mol. Biol. 102*, 27–59.

Eklund, H., Plapp, B. V., Samama, J.-P., & Brändén, C.-I. (1982a) *J. Biol. Chem. 257*, 14349–14358.

Eklund, H., Samama, J.-P., & Wallen, L. (1982b) *Biochemistry 21*, 4858–4866.

Eklund, H., Samama, J.-P., & Jones, T. A., (1984) *Biochemistry 23*, 5982–5996.

Goldstein, B. M., Takusagawa, F., Berman, H. M., Srivastava, P. C., & Robins, R. K. (1983) *J. Am. Chem. Soc. 105*, 7416–7422.

Goldstein, B. M., Takusagawa, F., Berman, H. M., Srivastava, P. C., & Robins, R. K. (1985) *J. Am. Chem. Soc. 107*, 1394–1400.

Goldstein, B. M., Mao, D. T., & Marquez, V. E. (1988) *J. Med. Chem. 31*, 1026–1031.

Goldstein, B. M., Bell, J. E., & Marquez, V. E. (1990a) *J. Med. Chem. 33*, 1123–1127.

Goldstein, B. M., Kennedy, S. D., & Hennen, W. J. (1990b) *J. Am. Chem. Soc. 112*, 8266–8268.

Goldstein, B. M., Leary, J. F., Farley, B. A., Marquez, V. E., Levy, P. C., & Rowley, P. T. (1991) *Blood 78*, 593–598.

Howard, A. J., Gilliland, G. L., Finzel, B. C., Poulos, T. L., Ohlendorf, D. H., & Salemme, F. R. (1987) *J. Appl. Crystallogr. 20*, 383–387.

IUPAC-IUB Joint Commission on Biochemical Nomenclature (JCBN) (1983) *Eur. J. Biochem. 131*, 9–15.

Jackson, R. C., Weber, G., & Morris, H. P. (1975) *Nature 256*, 331–333.

Jayaram, H. N. (1986) *Adv. Enzyme Regul. 24*, 67–89.

Jayaram, H. N., & Johns, D. G. (1986) *Biochem. Pharmacol. 35*, 3783–3790.

Jayaram, H. N., Ahluwalia, G. S., Dion, R. L., Gebeyehu, G., Marquez, V. E., Kelly, J. A., Robins, R. K., Cooney, D. A., & Johns, D. G. (1983) *Biochem. Pharmacol. 32*, 2633–2636.

Kabsch, W. (1988a) *J. Appl.* Crystallogr. *21*, 67–71.

Kabsch, W. (1988b) *J. Appl.* Crystallogr. *21*, 916–924.

Kiguchi, K., Collart, F. R., Henning-Chubb, C., & Huberman, E. (1990) *Exp. Cell. Res. 187*, 47–53.

Knight, R. D., Mangum, J., Lucas, D. L., Cooney, D. A., Khan, E. C., & Wright, D. G. (1987) *Blood 69*, 634–639.

Li, H., & Goldstein, B. M. (1992) *J Med. Chem. 35*, 3560–3567.

Lucas, D. L., Webster, H. K., & Wright, D. G. (1983) *J. Clin. Invest. 72*, 1889–1900.

Luzzati, P. V. (1952) *Acta Crystallogr. 5*, 802–881.

Marquez, V. E., Tseng, C. K. H., Gebeyehu, G., Cooney, D. A., Ahluwalia, G. S., Kelley, J. A., Dalal, M., Fuller, R. W., Wilson, Y. A., & Johns, D. G. (1986) *J. Med. Chem. 29*, 1726–1731.

Olah, E., Natsumeda, Y., Ikegami, T., Kote, Z., Horanyi, M., Szelenyi, J., Paulik, E., Kremmer, T., Hollan, S. R., Sugar, J., & Weber, G. (1988) *Proc. Natl. Acad. Sci. U.S.A. 85*, 6533–6537.

Ramachandran, G. N., & Sasisekharan, V. (1968) *Adv. Protein Chem. 23*, 283–437.

Reddy, B. S, Saenger, W., Muhlegger, K., & Weimann, G. (1981) *J. Am. Chem. Soc. 103*, 907–914.

Sack, J. S. (1988) *J. Mol. Graphics 6*, 224–225.

Samama, J.-P., Zeppezauer, E., Biellmann, J.-F., & Brändén, C.-I. (1977) *Eur. J. Biochem. 81*, 403–409.

Sidi, Y., Beery, E., Panet, L., Wasserman, A., Novogrodsky, A., & Nordenberg, J. (1989) *Eur. J. Cancer Clin. Oncol. 25*, 883–889.

Sokoloski, J. A., Blair, O. C., & Sartorelli, A. C. (1986) *Cancer Res. 46*, 2314–2319.

Steeter, D. R., & Robins, R. K. (1983) *Biochem. Biophys. Res. Commun. 115*, 544–550.

Tricot, G. J., Jayaram, H. N., Lapis, E., Natsumeda, Y., Nichols, C. R., Kneebone, P., Heerema, N., Weber, G., & Hoffman, R. (1989) *Cancer Res. 49*, 3696–3701.

Tricot, G. J., Jayaram, H. N., Weber, G., & Hoffman, R. (1990) *Int. J. Cell Cloning 8*, 161–170 and references therein.

Wright, D. G. (1987) *Blood 69*, 334–337.

Wu, Y. D., & Houk, K. N., (1991) *J. Am. Chem. Soc. 113*, 2353–2358.

Zeppezauer, E., Soderberg, B.-O., Brändén, C.-I., Akeson, A., & Theorell, H. (1967) *Acta Chem. Scand. 21*, 1099–1101.